PNAS RESEARCH ARTICLE | DEVELOPMENTAL BIOLOGY

Deficiency in glutathione peroxidase 4 (GPX4) results in abnormal lens development and newborn cataract

Zongbo Wei[a,1], Caili Hao[a,1], Kazi Rafsan Radeen[a], Zheng Hao[b], Kavitha Kettimuthu[c], Kristal Maner-Smith[c], Shinya Toyokuni[b], and Xingjun Fan[a,2]

Affiliations are included on p. 11.

Edited by Rachel W. Martin, University of California Irvine, Irvine, CA; received April 18, 2024; accepted October 3, 2024 by Editorial Board Member Krzysztof Palczewski

The human lens is composed of a monolayer of lens epithelial cells (LECs) and elongated fibers that align tightly but are separated by the plasma membrane. The integrity of the lens plasma membrane is crucial for maintaining lens cellular structure, homeostasis, and transparency. Glutathione peroxidase 4 (GPX4), a selenoenzyme, plays a critical role in protecting against lipid peroxidation. This study aims to elucidate the role of GPX4 in lens plasma membrane stability during lens development using in vitro, ex vivo, and in vivo systems. Our findings reveal that GPX4 deficiency triggers lens epithelial apoptosis-independent but ferroptosis-mediated cell death. Blocking lens GPX4 activity during ex vivo culture induces lens opacification, LEC death, and disruption of lens fiber cell arrangement. Deletion of lens-specific Gpx4 results in significant unsaturated phospholipid loss and an increase in oxidized phospholipids. Consequently, lenses with Gpx4 deficiency exhibit massive disruption of lens fiber cell structure, significant loss of LECs via ferroptosis, and formation of newborn cataracts. Remarkably, administering the lipid peroxidation inhibitor, liproxstatin-1, to pregnant mothers at embryonic days 9.5 significantly prevents lipid peroxidation, LEC death, and lens developmental defects. Our study unveils the crucial role of GPX4 in lens development and transparency, and also provides a successful intervention approach to prevent lens developmental defects through lipid peroxidation inhibition.

lipid peroxidation | GPX4 | cataract | ferroptosis | oxidation

Significance

Cataract is a leading cause of blindness worldwide, with multiple factors contributing to its formation. The lens is a remarkable tissue composed of a monolayer of epithelial cells and thousands of layers of fiber cells. The lens plasma membrane plays a crucial role in maintaining lens homeostasis and transparency. Substantial evidence suggests that lipid oxidation accumulates during lens aging, but the precise involvement of lipid peroxidation in lens cell fate and cataractogenesis remains unclear. Our research reveals that increased lipid peroxidation resulting from Glutathioneperoxidase 4 (GPX4) deficiency leads to damage to the lens plasma membrane and early-onset cataract. Remarkably, administration of a lipid peroxidation inhibitor significantly mitigates cataract formation—a phenomenon rarely observed in lens and cataract research.

Lens refractive power and transparency are intricately linked to the development and alignment of lens epithelial and fiber cells. The lens epithelium is formed by a monolayer of cuboidal lens epithelial cells (LECs), supported by numerous junction proteins, including cadherins, connexins, and tight junction proteins (1). These cells maintain lens homeostasis and transparency through their array of ion channels and transporters (2). Elongated lens fiber cells are produced through the differentiation of LECs. To optimize lens transparency and minimize light scattering, lens fiber cells undergo maturation, eliminating all cellular organelles, including mitochondria, lysosomes, and the nucleus (3). The inner layers of the lens, including the lens nucleus, constitute the organelle-free zone, with fiber cell subcellular structures, such as cytoplasm and cytoskeleton, enclosed by a plasma membrane.

The stability and integrity of the lens plasma membrane are crucial for maintaining lens homeostasis and transparency. Biological membranes rely on their ability to act as barriers against the permeation of polar molecules for their integrity and functionality (4). These membranes mainly comprise highly saturated phospholipids (PLs), with approximately 66% being sphingomyelins (SMs) and dihydro SMs. The saturation of PLs, particularly SMs, leads to membranes with low hydrophobicity at the center, while the addition of cholesterol (Chol), constituting 30 to 50 mol%, is essential for maximal hydrophobicity (5). The lens plasma membrane also contains substantial levels of unsaturated PLs, such as phosphatidylethanolamine (PE) and phosphatidylcholine (PC), which contribute to structural integrity and modulation of fluidity (6). Their dynamic interactions with other lipids, proteins, and small molecules play vital roles in maintaining lens cellular and lens homeostasis.

Unsaturated lipids, like glycerophospholipids, are vulnerable to lipid peroxidation, a process where free radicals steal electrons from cell membrane lipids, resulting in cell damage (7). This is because oxidized PLs can often bring profound changes in biological activities. With aging, levels of highly unsaturated lipids, like glycerophospholipids, decline, while levels of highly saturated lipids, like sphingolipids, increase in the human lenses (8). The steep decline of highly unsaturated glycerophospholipids, especially PE-like

Author contributions: X.F. designed research; Z.W., C.H., K.R.R., Z.H., K.K., K.M.-S., S.T., and X.F. performed research; Z.W., C.H., K.R.R., K.K., K.M.-S., and X.F. analyzed data; Z.H. and S.T. contributed new reagents/analytic tools; and X.F. wrote the paper.

The authors declare no competing interest.

This article is a PNAS Direct Submission R.W.M. is a guest editor invited by the Editorial Board.

Copyright © 2024 the Author(s). Published by PNAS. This article is distributed under Creative Commons Attribution-NonCommercial-NoDerivatives License 4.0 (CC BY-NC-ND).

[1]Z.W. and C.H. contributed equally to this work.

[2]To whom correspondence may be addressed. Email: xfan@augusta.edu.

This article contains supporting information online at https://www.pnas.org/lookup/suppl/doi:10.1073/pnas.2407842121/-/DCSupplemental.

Published November 19, 2024.

lipids (9), in the lens is believed to result from selective lipid peroxidation. Furthermore, there is substantial evidence supporting the presence of lipid peroxidation in the human lens. Babizhayev (10) detected lipid peroxidation products in the aqueous humor of patients with senile and complicated cataracts, Borchman et al. (11) measured the increasing lipid oxidation of PLs with age in human lenses via infrared spectroscopy. Specifically, direct lipid peroxidation product malondialdehyde (MDA) levels are significantly higher in aged and cataractous human lenses (11).

A cellular defense system to counter lipid peroxidation involves a combination of antioxidants, enzymes, and repair mechanisms. Glutathione peroxidase 4 (GPX4) is an intracellular selenoperoxidase. First isolated from pig liver (12), GPX4 detoxifies the phospholipid hydroperoxides, peroxidation of cholesterol, and cholesterol-ester hydroperoxides, at the expense of GSH, even when hydroperoxides are present in biomembranes or lipoproteins (13). GPX4 plays a vital role in maintaining cell membrane integrity and protecting cells from oxidative damage. GPX4 has been implicated in various diseases, including neurodegenerative disorders (14), cancer (15), cardiovascular diseases (16), and ischemia–reperfusion injury (17). Mice lacking GPX4 die early in embryogenesis (18), further proving the essential role of GPX4 in cellular function. Our previous study demonstrated that the aging lens epithelium is highly susceptible to ferroptosis when GPX4 activity is inhibited, suggesting that the aging lens possesses all necessary factors to promote ferroptosis (19). Ma et al. (20) confirmed the existence of ferroptosis in lens epithelium from age-related cataract patients using electron microscopy (EM). Recently, several lncRNAs have been found to regulate GPX4 and ferroptosis in in vitro LEC culture models (21, 22). However, the role of GPX4 in lens biology and aging remains largely unexplored. In this study, we reveal the critical function of GPX4 in lens development and cataractogenesis using in vitro, ex vivo, and in vivo models.

Results

GPX4 Is Crucial for the Survival of LECs. To explore the role of GPX4 in LECs, we generated GPX4 knockout (KO) FHL124 LECs using the CRISPR/Cas9 method. Throughout the selection process, 50 nM liproxstatin-1 (Lip-1) was supplemented in the culture medium. Two clones (CL-11 and CL-15) exhibiting no detectable GPX4 were utilized for this investigation. Cell viability was assessed upon Lip-1 removal from the culture medium. As depicted in Fig. 1*A*, significant cell death was evident in GPX4 KO cells compared to the wild type (WT) 24 h after Lip-1 withdrawal. GPX4 KO cells maintained in the presence of Lip-1 exhibited comparable cell viability to WT cells (Fig. 1*A*). Given GPX4's crucial role in preserving plasma membrane integrity, we quantified the release of lactate dehydrogenase (LDH), a marker indicative of plasma membrane damage. As illustrated in Fig. 1*B*, both CL-11 and CL-15 cells displayed a notable increase in LDH release compared to WT cells.

Using the BODIPY 581/591 C11 lipid peroxidation sensor, we detected heightened plasma membrane lipid peroxidation in GPX4 KO cells 24 h post Lip-1 removal (Fig. 1 *C*–*K* and *U*). Consistently, we observed pronounced 4-hydroxynonenal (HNE)-positive IF staining, indicative of elevated lipid peroxidation status, in GPX4 KO LECs relative to WT cells (Fig. 1 *L*–*U*). Immunoblotting further confirmed increased HNE production in GPX4 KO cells compared to WT cells (Fig. 1*V*). Notably, we detected a range of protein bands because the HNE antibody recognizes any protein carrying HNE conjugation, primarily through Michael addition. Moreover, the intracellular iron concentration was significantly elevated in GPX4 KO cells relative to WT (Fig. 1*W*), suggesting that iron-mediated lipid peroxidation might underlie the mechanism of LEC cell death.

The Cytosolic Isoform of GPX4 (cGPX4) Is Predominantly Expressed in LECs. GPX4 has three isoforms: cytosolic (cGPX4), mitochondrial (mGPX4), and nuclear (nGPX4), typically exhibiting tissue-specific distributions (23). We assessed the expression levels of GPX4 in all three cellular compartments of FHL124 cells and observed that cytosolic GPX4 was the most abundant form, with substantial levels also detected in mitochondria, while no detectable nuclear GPX4 was observed (*SI Appendix*, Fig. S1*A*). To validate the absence of nGPX4 in FHL124 cells, we utilized mouse epididymis lysate, known for its high nGPX4 expression. As illustrated in *SI Appendix*, Fig. S1*B*, nGPX4 was indeed detected in the epididymis, appearing at approximately 25 kDa, whereas negligible levels were observed in FHL124 cells. Subsequently, we investigated the cellular functions of cGPX4 and mGPX4. In *SI Appendix*, Fig. S1*C*, upon overexpression of cGPX4 and mGPX4 in WT FHL124 cells, both cytosolic and mitochondrial GPX4 effectively rescued cells from cell death induced by RSL3, a GPX4 inhibitor. In a parallel experiment, we introduced cGPX4 and mGPX4 into GPX4 KO FHL124 cells and observed similar rescue effects, indicating that both isoforms could mitigate cell death resulting from GPX4 deficiency (*SI Appendix*, Fig. S1 *D*–*T*).

Blocking GPX4 Activity in Ex Vivo Lens Culture Disrupts Fiber Cell Organization and Induces Lens Opacity. Given the vital role of GPX4 in LECs' survival, we sought to investigate its biological function within the lens. We conducted ex vivo cultures of 2-mo-old mouse lenses for 2 wk in M199 medium without serum. In WT lenses, the majority remained transparent (Fig. 2*A*). However, the presence of 10 μM (1S, 3S)-RSL3 (RSL3) led to opacity development in almost all lenses (Fig. 2*B*). Notably, opacity was pervasive throughout the entire lens posttreatment, with denser opacity observed in the lens nucleus (Fig. 2*B*). Histological sections revealed a shift from the classical hexagonal profile to a round fiber cell morphology in RSL3-treated lenses within the cortical region (Fig. 2*C*). Additionally, a decrease in epithelial cells was observed in the epithelium of RSL3-treated lenses compared to nontreated controls (Fig. 2*C*). IF staining with Wheatgerm agglutinin (WGA)-Rhodamine, a membrane-specific marker, demonstrated disrupted fiber structure with a round shape profile in RSL3-treated lenses, contrasting with the well-organized fiber alignment in nontreated lenses (Fig. 2*D*).

Further analysis of lens iron levels revealed a significant increase in iron content in RSL3-treated lenses compared to nontreated controls (Fig. 2*E*). As anticipated, lipid peroxidation products HNE and malondialdehyde (MDA) were both significantly elevated in RSL3-treated lenses compared to nontreated lenses (Fig. 2 *F* and *G*). These findings collectively indicate that blocking GPX4 activity in ex vivo cultured lenses induces plasma membrane lipid peroxidation, cell death, and disruption of fiber cell alignment.

Lens-Specific Conditional Gpx4 Deletion Induces Newborn Cataract and Microphthalmia. Subsequent to these findings, we generated a lens-specific conditional Gpx4 KO mouse model through the crossbreeding of Gpx4 floxed mice with MLR10-Cre mice, which express Cre specifically in the lens at embryonic day 10.5 (E10.5). Intriguingly, newborn cataract formation was observed in lens-conditional Gpx4 KO ($Gpx4^{-/-}$) mice (Fig. 3*B*, with WT slit lamp image shown in Fig. 3*A*). Dissection of lenses further revealed cataract formation in lens Gpx4 deficient mice (Fig. 3*C*), with abnormal lens fiber structure

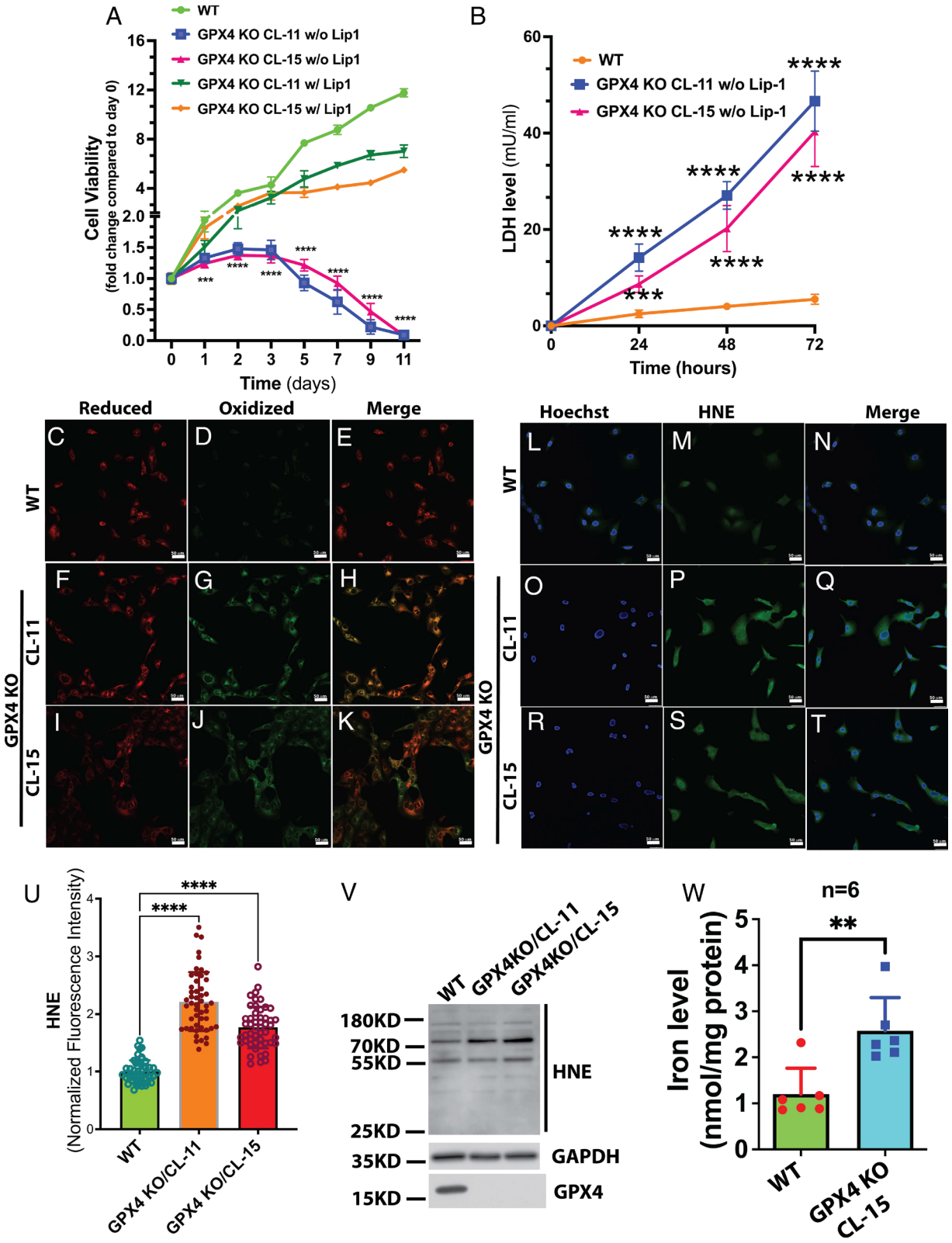

Fig. 1. GPX4 deletion induces plasma membrane lipid peroxidation and cell death in LECs. FHL124 LECs were subjected to analysis with or without GPX4 to evaluate cell viability, iron levels, and plasma membrane lipid peroxidation. (*A*) Two distinct GPX4 KO clones of FHL124 cells exhibited significant decreases in cell viability in the absence of Lip-1 in the culture medium compared to WT cells and Lip-1 treated GPX4 KO cells. (*B*) A significantly elevated LDH level was observed in the culture medium of GPX4 KO cells without Lip-1 compared to WT cells. (*C–K*) C11-Bodipy labeling assay revealed a marked increase in lipid peroxidation in the cell membranes of both clone 11 (CL-11) and clone 15 (CL-15) GPX4 KO cells compared to WT cells. (*L–U*) HNE IF staining indicated enhanced formation of 4-hydroxynonenal (HNE) in GPX4 KO cells relative to WT cells in both clone 11 and clone 15. Quantitative data are presented in *U*. (*V*) Immunoblotting analysis also demonstrated increased HNE formation in GPX4 KO cells compared to WT cells in both CL11 and CL15. (*W*) Intracellular iron levels were significantly elevated in GPX4 KO cells compared to WT cells. Two-way ANOVA with Tukey's multiple comparisons and Sidak's multiple comparisons tests were conducted for *A* and *B*, respectively. Ordinary one-way ANOVA with Tukey's multiple comparisons test was performed for *U*, and an unpaired *t* test was conducted for *W*. Significance was considered at $P < 0.05$, denoted as *<0.05, **<0.01, ***<0.001, ****<0.0001.

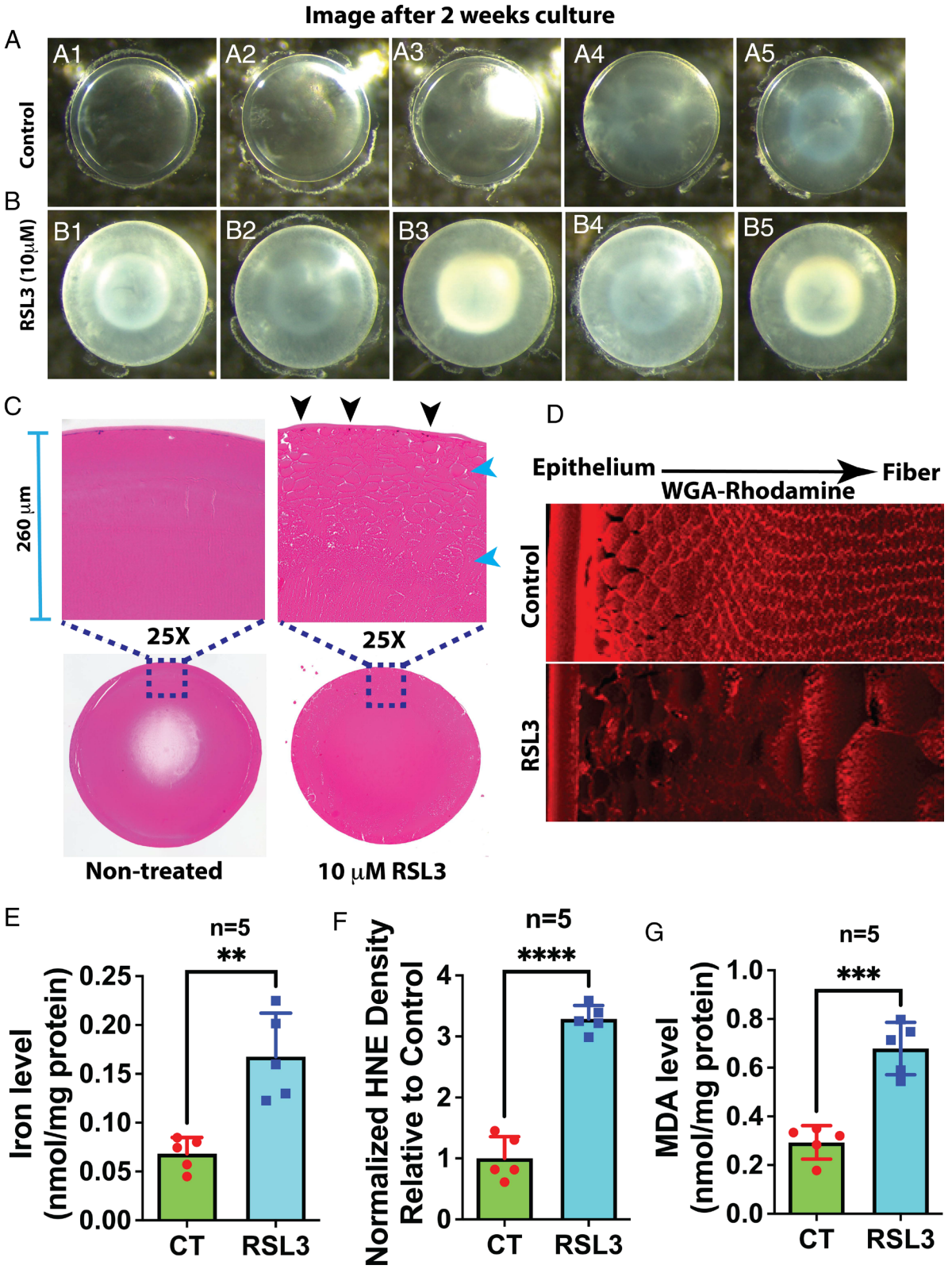

Fig. 2. Inhibition of GPX4 activity induces lens opacity in ex vivo lens culture. Lenses from 2-mo-old mice were cultured in M199 medium for 2 wk with or without the presence of 10 μM RSL3, followed by analysis. (*A*) The majority of lenses without RSL3 treatment remained transparent (A1 to A5, five biological replicates). (*B*) All lenses treated with RSL3 developed opacity (B1 to B5, five biological replicates). (*C*) Round-shaped fiber cells were observed in RSL3-treated lenses within the cortical fiber layer, contrasting with the elongated fiber alignment seen in nontreated lenses. (*D*) WGA-Rhodamine staining revealed round and disrupted fiber shapes in RSL3-treated lenses, while nontreated lenses exhibited flat and hexagonal fiber alignment. (*E*) Significantly increased iron levels were detected in RSL3-treated lenses compared to nontreated lenses. (*F*) There was a significant elevation in HNE formation in RSL3-treated lenses compared to nontreated lenses. (*G*) RSL3-treated lenses exhibited significantly increased MDA formation compared to nontreated lenses. Unpaired *t* tests were performed for *E*–*G*. Significance was considered at $P < 0.05$, denoted as *<0.05, **<0.01, ***<0.001, ****<0.0001.

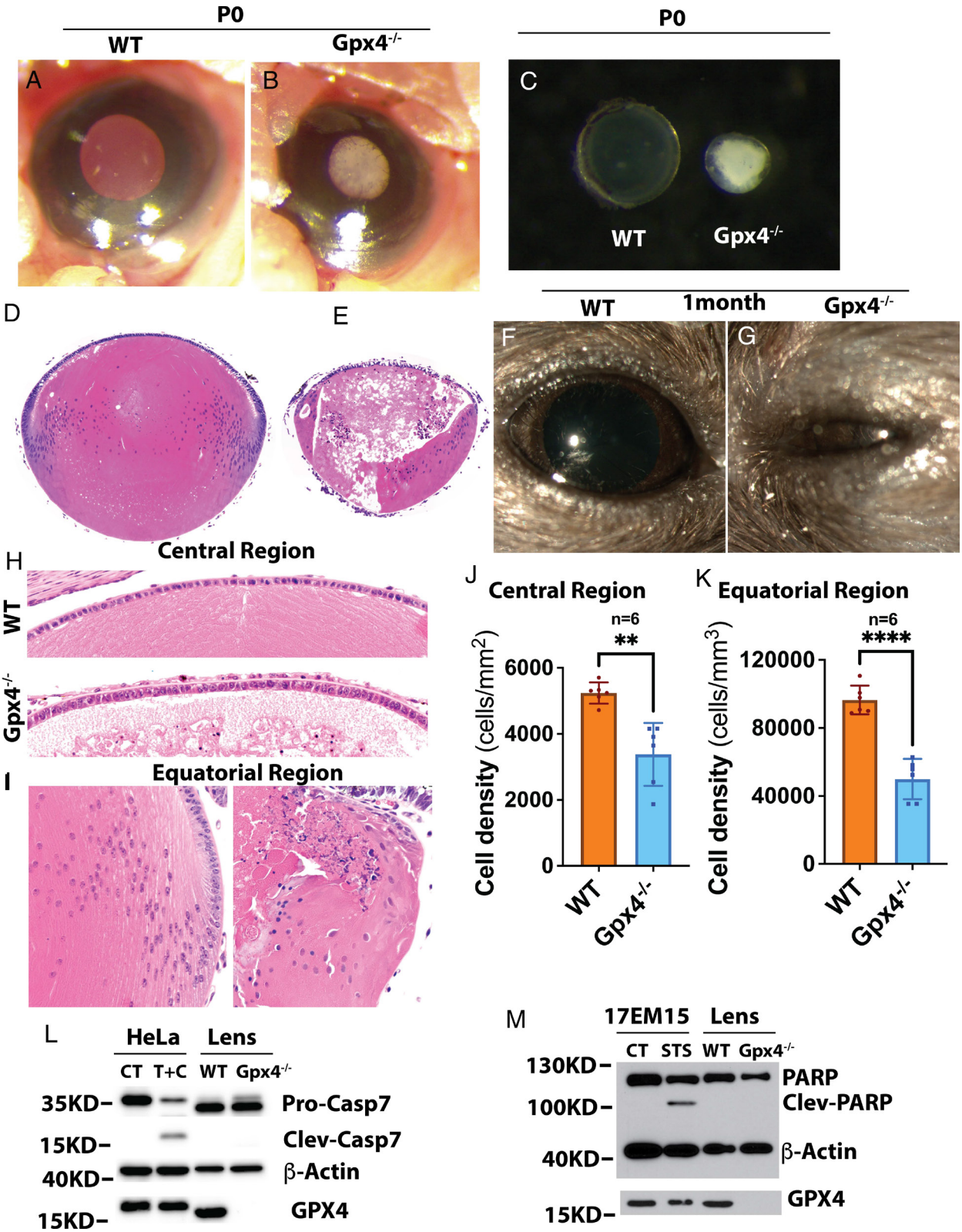

Fig. 3. Lens-specific Gpx4 deletion induces cell death, newborn cataract formation, and microphthalmia. Lens-specific Gpx4 deletion was achieved through crossbreeding between MLR10-Cre and Gpx4 floxed ($Gpx4^{f/f}$) mice. Only mice with a high level of Gpx4 deletion were used for comparison with control mice in the studies. (*A* and *B*) Slit lamp images of newborn mice revealed dense cataract formation in Gpx4 KO mice ($Gpx4^{-/-}$) (*B*) compared to clear WT mice (*A*). (*C*) Darkfield images of lenses displayed dense opacity in $Gpx4^{-/-}$ mice. (*D* and *E*) H&E staining depicted disrupted lens fiber structure in $Gpx4^{-/-}$ lenses. (*F* and *G*) $Gpx4^{-/-}$ mice exhibited microphthalmia at 1 mo of age (*G*) compared to normal eye morphology in WT mice (*F*). (*H*) Representative image of the central region of WT and $Gpx4^{-/-}$ lenses. (*I*) Representative image of the equatorial region of WT and $Gpx4^{-/-}$ lenses. (*J*) Significant loss of epithelial cells in the central region of $Gpx4^{-/-}$ lenses as evidenced by cell counts. (*K*) Significant loss of epithelial cells in the equatorial region of $Gpx4^{-/-}$ lenses as evidenced by cell counts. (*L*) Immunoblotting assay revealing no cleavage caspase 7, with TNFα plus cycloheximide (T+C) treated HeLa cells serving as a positive control. (*M*) The immunoblotting assay showed no cleavage poly (ADP-ribose) polymerase (PARP), with staurosporine-treated mouse LECs 17EM15 as a positive control. Unpaired *t* tests were conducted for *J* and *K*. Significance was considered at $P < 0.05$, indicated as *<0.05, **<0.01, ***<0.001, ****<0.0001.

evident in Hematoxylin and eosin (H&E) staining (Fig. 3 *D* and *E*). Subsequent observations indicated that lens-specific Gpx4 deletion led to microphthalmia (Fig. 3 *F* and *G*). Consistent with expectations, visual acuity measurement demonstrated almost no detectable visual ability in Gpx4$^{-/-}$ mice (*SI Appendix*, Fig. S2).

Interestingly, during our study, we sometimes observed varying phenotypes among Gpx4 KO mice. Some displayed a less severe phenotype, while others exhibited no lens phenotype. We collectively monitored 99 mice up to the age of 2 mo and noted varying degrees of lens opacity. As depicted in *SI Appendix*, Fig. S3, approximately 79% of the mice exhibited severe lens phenotype and microphthalmia (*SI Appendix*, Fig. S3 *B* and *C*), around 14% displayed lens opacity with relatively normal eye size (*SI Appendix*, Fig. S3 *D* and *E*), and 8% showed no lens phenotype. Upon examining lens GPX4 protein expression, we confirmed efficient GPX4 deletion in mice with lens cataract phenotype, whereas mice without lens phenotype exhibited almost no GPX4 deletion (*SI Appendix*, Fig. S4*A*). This prompted us to investigate recombinant Cre expression in these mice lenses. As illustrated in *SI Appendix*, Fig. S4*A*, mice with lens opacity phenotype displayed recombinant Cre expression in the lens extract, whereas no Cre was detected in Gpx4 KO mice without lens phenotype. Genotype analysis confirmed the presence of correct Cre and Gpx4 floxed gene in all mice (*SI Appendix*, Fig. S4*B*).

To further investigate Cre mosaicism phenomena, we conducted a comparative analysis of Cre and GPX4 protein expression in P0 lenses. As depicted in *SI Appendix*, Fig. S5, MLRCre/Gpx4floxed mice, confirmed through PCR genotyping analysis, exhibited varying levels of Cre and GPX4 protein within the lens: some displayed no detectable GPX4, others exhibited markedly reduced levels compared to Gpx4 floxed mice lenses, while some demonstrated nearly identical levels of GPX4 protein expression. Consistent with expectations, the level of Cre expression inversely correlated with GPX4 protein expression. These findings suggest that the absence of a lens opacity phenotype in certain mice corresponds to the lack of recombinant Cre expression, implying that complete Gpx4 deletion is linked with 100% penetrance in lens cataract formation.

Due to the phenomenon of Cre mosaicism, we limited our comparisons to highly Gpx4-deleted mice with control mice in several of our studies, including slit-lamp imaging, lens dark field imaging, immunohistochemistry (IHC), electron microscopy (EM), and histology. In these cases, one eye was used to determine Cre and GPX4 expression. However, for lens lipidomics and rescue studies, a large number of animals were used, and lenses were collected based solely on the correct genotype.

To track the progression of abnormal lens development, we conducted histological examinations of the lens at various embryonic stages: embryonic days 12.5 (E12.5), E13.5, E14.5, E15.5, E16.5, and E18.5. Due to Cre mosaicism, we analyzed at least five Gpx4f/f embryos (control) and at least 10 Gpx4 KO embryos. The number of lenses exhibiting the phenotype at each time point is shown in *SI Appendix*, Table S2. As illustrated in *SI Appendix*, Fig. S6 *A–L*, no noticeable pathology was evident at E12.5, E13.5, and E14.5. However, a clear vacuole appeared in the germinative zone at E15.5 (*SI Appendix*, Fig. S6 *G* and *H* and *Insets*), which then expanded further by E16.5 (*SI Appendix*, Fig. S6 *I* and *J*). By E18.5, a severe disruption in fiber cell organization was observed (*SI Appendix*, Fig. S6 *K* and *L*). Postnatally, we continued monitoring lens degeneration by examining histological sections at P5, P10, P15, P20, P30, and P90. As shown in *SI Appendix*, Fig. S3 *M–X*, significant lens degeneration occurred within the initial two weeks (*SI Appendix*, Fig. S6 *M–R*), resulting in only a small fragment of disorganized lens tissue remaining thereafter (*SI Appendix*, Fig. S6 *S–X*).

Gpx4 Deletion Induces Apoptosis-independent Cell Death in LECs. Upon examination of the LECs in both central and equatorial regions, we observed cell loss in Gpx4 KO lenses. We developed separate methods to count cell numbers in both regions. For the central region, we counted epithelial cells in a series of contiguous sections and calculated the cell number per area (Fig. 3*H*). For the equatorial region, we counted epithelial cells by nuclei staining of a series of contiguous sections and calculated the cell density by the number of cells per volume (Fig. 3*I*). As shown in Fig. 3 *J* and *K*, a significant loss of epithelial cells was observed in both the central and equatorial regions of the lens in Gpx4 KO mice compared to WT mice. We further confirmed cell death by propidium iodide (PI) staining, a cell death marker. We observed elevated PI-positive stained cells throughout the entire lens epithelium, including the bow region, where LECs elongate into fiber cells (*SI Appendix*, Fig. S7 *D–F*), while no detectable PI-positive staining was found in WT lenses (*SI Appendix*, Fig. S7 *A–C*).

To examine whether LEC death occurred through an apoptotic-mediated mechanism, we performed immunofluorescence (IF) staining to detect cleaved caspase 3, an apoptosis marker. However, we could not detect cleaved caspase 3 in WT and Gpx4 KO lens epithelium (*SI Appendix*, Fig. S7 *I–L*). To validate the IF staining method, we used lenses from UVB-irradiated mice, which we have previously shown induced LEC apoptosis (24). As shown in *SI Appendix*, Fig. S7 *G* and *H*, a significant number of LECs showed positive cleaved caspase 3 staining from lenses collected on day 4 after a dose of 11.20 kJ/m^2 ultraviolet B (UVB) exposure. To confirm that apoptosis is not part of the cell death mechanism in Gpx4 KO lenses, we performed immunoblotting assays measuring cleaved caspase 7 and PARP, markers of apoptosis. As shown in Fig. 3 *L* and *M*, no cleaved caspase 7 and PARP were detected in Gpx4 KO lenses. Both TNFα plus cycloheximide (T+C) and staurosporine induced cell apoptosis were used as positive controls. Notably, when comparing cells with lens tissue, we observed different band intensities of the internal control β-actin, despite loading equal amounts of protein, as confirmed by Ponceau staining (*SI Appendix*, Fig. S8). Taken together, these data suggest that GPX4 deficiency-mediated LEC death is independent of cell apoptosis.

GPX4 Deficiency Induces Lipid Peroxidation and Ferroptosis. Given that GPX4 serves as a crucial detoxification enzyme for lipid peroxide, we evaluated two small molecule lipid peroxidation products, HNE and MDA. An immunoblotting assay employing an HNE antibody revealed a substantial increase in HNE formation in Gpx4 KO lenses compared to WT, as shown in Fig. 4*A*. Additionally, IHC staining, utilizing a highly specific and sensitive HNE antibody developed by Toyokuni's group (25), illustrated a profound increase in HNE levels in Gpx4 KO lenses relative to WT, as depicted in Fig. 4*B*, with quantified data presented in Fig. 4*C*. Similarly, we observed significantly elevated MDA formation in Gpx4 KO lenses compared to WT (Fig. 4*D*).

To gain a comprehensive understanding of lens plasma membrane PLs, we conducted lipidomic analysis via LC–MS/MS, measuring both PLs and oxidized PLs in E18.5 embryonic lenses. A total of 456 WT and 549 Gpx4 KO embryonic lenses were harvested and randomly distributed across 4 biological replicates, each with an average wet weight of 32 mg per sample. Principal component analysis distinctly illustrated the differing profiles of plasma membrane PLs (Fig. 4*E*). As depicted in the heatmap (Fig. 4*F*), a notable decrease in the levels of numerous PE, PC, phosphatidic acids (PA), and phosphatidylglycerol (PG) species was observed in Gpx4 KO lenses compared to WT. For example, PE 34:1 exhibited a significant decrease ($P = 0.0479$) in Gpx4 KO

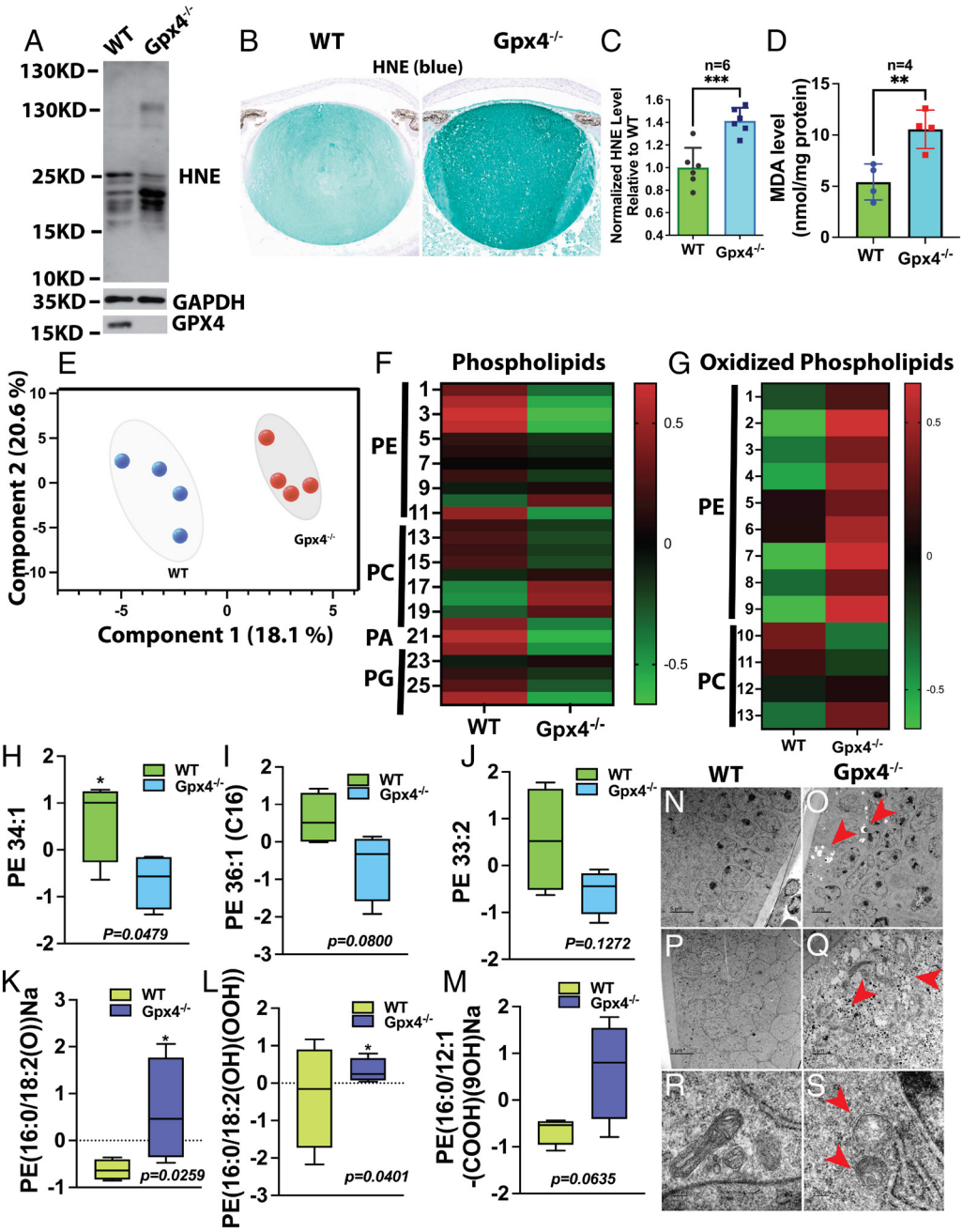

Fig. 4. Gpx4 deficient lenses manifested with increased lipid peroxidation, reduced PLs, increased oxidized PLs, and induced mitochondrial damage. (*A*) Immunoblotting assay indicating increased HNE formation in Gpx4$^{-/-}$ mouse lenses compared to WT. (*B*) IHC staining using the HNEJ-1 antibody revealed significantly elevated HNE staining in Gpx4$^{-/-}$ mouse lenses, with HistoGreen substrate employed. (*C*) Quantitative data from IHC staining demonstrating a significant rise in HNE formation in Gpx4$^{-/-}$ mouse lenses. (*D*) Lipid peroxidation product MDA showing a significant increase in Gpx4$^{-/-}$ mouse lenses compared to WT. (*E*) Principal component analysis (PCA) demonstrating distinct changes in phospholipid composition based on phospholipid liquid chromatography with tandem mass spectrometry (LC–MS/MS) analysis. (*F*) Heat map indicating a reduction in PLs in Gpx4$^{-/-}$ mouse lenses compared to WT. (*G*) Heat map illustrating increased levels of oxidized PLs in Gpx4$^{-/-}$ mouse lenses compared to WT. (*H*) Significantly lower levels of PE 34:1 were observed in Gpx4$^{-/-}$ mouse lenses compared to WT. (*I* and *J*) PE 36:1 (C16) and PE 33:2 showed a trend toward reduced levels in Gpx4$^{-/-}$ mouse lenses compared to WT, although statistical significance was not reached. (*K* and *L*) PE (16:0/18:2(O))Na and PE (16:0/18:2(OH)(OOH)) exhibiting a significant increase in Gpx4$^{-/-}$ mouse lenses compared to WT. (*M*) PE (16:0/12:1(COOH)(9OH))Na showing a trend toward increased levels in Gpx4$^{-/-}$ mouse lenses compared to WT, although statistical significance was not achieved. (*N* and *O*) Transmission EM (TEM) exhibited multiple vacuoles near-equatorial regions in Gpx4$^{-/-}$ mouse lenses (*O*) compared to WT lenses (*N*). (*P* and *Q*) Noticeable lipid droplets were observed in Gpx4$^{-/-}$ mouse lenses (*Q*) compared to WT lenses (*P*). (*R* and *S*) Profound loss of mitochondrial cristae was evident in Gpx4$^{-/-}$ mouse lenses compared to WT. For panel *A–D* and *N–S* only mice with a high level of Gpx4 deletion were used for comparison with control mice. For panel *E–M*, all mice with correct Gpx4 KO genotype were used for comparison with control mice. Unpaired *t* tests were conducted for *C*, *D*, and *H–M*. Significance was considered at $P < 0.05$, denoted as *<0.05, **<0.01, ***<0.001, ****<0.0001.

lenses compared to WT, while PE 36:1 and PE 33:2 displayed a trend of lower levels in Gpx4 KO lenses relative to WT, albeit not statistically significant (Fig. 4 *H–J*). Conversely, elevated levels of oxidized PLs, particularly oxidized PE, were detected in Gpx4 KO lenses compared to WT (Fig. 4*G*). Notably, significant increases were observed in phospholipid oxidation products, including PE(16:0/18:2(O))Na ($P = 0.0259$) and PE(16:0/18:2(OH)(OOH)) ($P = 0.0401$), with a trending increase in PE(16:0/12:1 (COOH)(9OH)Na ($P = 0.0635$) in Gpx4 KO lenses relative to WT (Fig. 4 *K–M*). These findings strongly indicate that GPX4 deficiency induces lipid peroxidation, consequently altering the composition of plasma membrane lipids.

The heightened levels of lipid peroxidation products prompted us to investigate the role of ferroptotic-mediated cell death. *SI Appendix*, Fig. S9*A* reveals a significantly higher concentration of iron in Gpx4 KO lenses compared to WT. Furthermore, we measured several markers associated with ferroptosis. As shown in *SI Appendix*, Fig. S9*B*, the transferrin receptor 1 (TfR1) and acyl-CoA synthetase long-chain family member 4 (ACSL4) exhibited increases in expression in Gpx4 KO lenses compared to WT. Additionally, protein expression levels of cysteine-glutamate antiporter (xCT) and ferritin light chain (FTL) were elevated in Gpx4 KO lenses relative to WT. To comprehend the ultrastructural changes induced by GPX4 deficiency, transmission EM (TEM) was performed. Fig. 4 *N* and *O* demonstrate vacuolization in the lenses of Gpx4 KO mice near the equatorial region. Notably, lipid droplets were observed in Gpx4 KO lenses but not in WT lenses (Fig. 4 *P* and *Q*). Importantly, a profound decrease in mitochondrial cristae was evident in Gpx4 KO lenses compared to WT (Fig. 4 *R* and *S*). These data suggest that ferroptosis plays a vital role in LEC death and cataract formation.

Blocking Lipid Peroxidation Can Significantly Ameliorate Lens Developmental Defects. To validate the crucial role of GPX4 in safeguarding against lipid peroxidation during lens development, we conducted rescue experiments by administering the lipid peroxidation inhibitor, Lip-1, daily to pregnant mothers at both embryonic days 9.5 (E9.5) and E12.5, referred to as Rescue-1 (Res-1) and Rescue-2 (Res-2), respectively, as depicted in Fig. 5*A*. Mouse litter lens analysis was performed on the day after birth (P0). As illustrated in Fig. 5*B*, compared to the newborn cataract lenses in nontreated Gpx4 KO mice, both Res-1 and Res-2 markedly restored lens size and transparency in Lip-1 treated Gpx4 KO mothers compared to $Gpx4^{f/f}$ control mice. Slit lamp images shown in Fig. 5 *C*–*F* depicted opaque lens images of nontreated Gpx4 KO mice and transparent lens images of both Res-1 (Fig. 5*E*) and Res-2 (Fig. 5*F*) compared to $Gpx4^{f/f}$ control mice (Fig. 5*C*). Similarly, H&E staining demonstrated normal lens morphology in both Res-1 and Res-2 litters compared to $Gpx4^{f/f}$ control litters (Fig. 5 *G*–*J*). Overall, administration of Lip-1 at E9.5 significantly ($P < 0.05$) rescued lens developmental defects (Fig. 5*K*). However, administration at E12.5 resulted in an increased rate of cataract-free lenses compared to vehicle treatment, although this difference did not reach statistical significance (Fig. 5*K*). We further analyzed LEC numbers in both central and equatorial regions and found that Lip-1 administration at both E9.5 (Res-1) and E12.5 (Res-2) largely prevented LEC death compared to nontreated Gpx4 KO lenses (Fig. 5 *L* and *M*). WGA-Rhodamine staining revealed disrupted fiber arrangement in nontreated Gpx4 KO lenses at P0 (Fig. 5*O*) compared to Gpx4f/f control mice lenses (Fig. 5*N*). Lip-1 administration at both E9.5 (Res-1) and E12.5 (Res-2) significantly restored lens fiber structure and morphology (Fig. 5 *P* and *Q*). Consistently, the lipid peroxidation product HNE was significantly reduced in Res-1 and Res-2 treated mice lenses compared to nontreated Gpx4 KO mice lenses (Fig. 5*R*). These results strongly indicate that GPX4 is essential in lens development by preventing lipid peroxidation.

Discussion

In our current investigation, employing a combination of in vitro, ex vivo, and in vivo models, we elucidated the critical role of GPX4 in preserving the integrity of the lens plasma membrane and maintaining lens transparency. Our findings illustrate that GPX4 deficiency can exacerbate lipid peroxidation and lead to damage in the lens plasma membrane, ultimately triggering apoptosis-independent but ferroptosis-related cell death. This form of cell death is implicated in the development of newborn cataracts. Importantly, our study shows that preventing lipid peroxidation during the embryonic stage can mitigate lens developmental abnormalities and prevent cataract formation.

The lens membrane is essential for maintaining homeostasis, transparency, and refractive properties by acting as an impermeable barrier to cations and providing support for integral membrane proteins such as aquaporin-0 (AQP0) (26), ion pumps (27), and connexins (28). The integrity of the lens membrane affects fluidity and cell organization (5), particularly within the mature fibers, where the plasma membrane is the sole subcellular component. Lens fiber junctions are closely associated with their lipid environment. Studies involving lens fiber junction isolation and purification have shown an enrichment of lipids in these junctions across various species, including bovine (29), rat (30), chicken (31), and human lenses (30). For instance, in isolated bovine lens junctional membranes, phospholipid levels increased by 99-fold, and cholesterol levels surged by 144-fold compared to total lens plasma membranes (29). Using cryogenic electron microscopy (Cryo-EM), Flores et al. (32) demonstrated that the local lipid environment plays a crucial role in stabilizing and facilitating gap junctions, such as Cx46/50. Crystallography studies have shown that lipid molecules are required for the proper packing of junctional AQP0 tetramers, another key lens fiber junction protein (33). Moreover, connexins and AQP0 can assemble into supramolecular complexes, a process that necessitates the presence of local lipids to facilitate complex formation (34). Interestingly, numerous studies have demonstrated that lipid peroxidation and its products, such as HNE, can modulate the functions of cellular junctions through various cell signaling pathways, including the induction of endothelial barrier dysfunction (35, 36). Atomistic molecular dynamics simulations have shown that lipid oxidation significantly impacts connexin 26 hemichannel stability and function (37). However, the role of lipid peroxidation and changes in plasma lipid profiles in the structure, stability, assembly, and function of lens adherens and adhesion junctions remains unexplored. Targeting GPX4 activity, such as using lens-specific Gpx4-deficient mouse models, may serve as a valuable tool for investigating these questions.

Oxidation is considered a major cause of the loss of unsaturated PLs. Despite low oxygen levels, the human lens undergoes photo- and/or chemical oxidation, affecting both lipids and proteins (38). MDA, a byproduct of lipid oxidation, increases with age and cataract development (11). Our study supports the notion that oxidation-mediated loss of PLs, such as PE, PC, PA, and PG, occurs when lipid peroxidation detoxifying enzymes are deficient in the lens. Conversely, oxidized PLs are elevated in Gpx4 deficient lenses.

Both GPX1 and GPX4 are highly expressed in the lens epithelium and fiber cells (39). GPX1 functions as a cytosolic antioxidant enzyme, mitigating oxidative damage by catalyzing the reduction of hydrogen peroxide using GSH as a cofactor. Somatic GPX1 KO mice exhibit lens opacity between 6 to 9 mo of age, progressing to mature cataracts beyond 12 to 15 mo (40, 41). The delayed onset of cataract formation can be attributed to the presence of various antioxidant enzymes and molecules in the lens, such as catalase, which also aid in the removal of hydrogen peroxide (42–44). In contrast, GPX4 serves as the sole intracellular selenoperoxidase, to detoxify lipid hydroperoxides (13, 45, 46). Our current study suggests that GPX4 deficiency initiated at E10.5 can induce profound cell death and cataract formation. Our investigations, spanning in vitro, ex vivo, and in vivo approaches, collectively propose ferroptosis as the mechanism underlying LEC death associated with elevated iron levels and

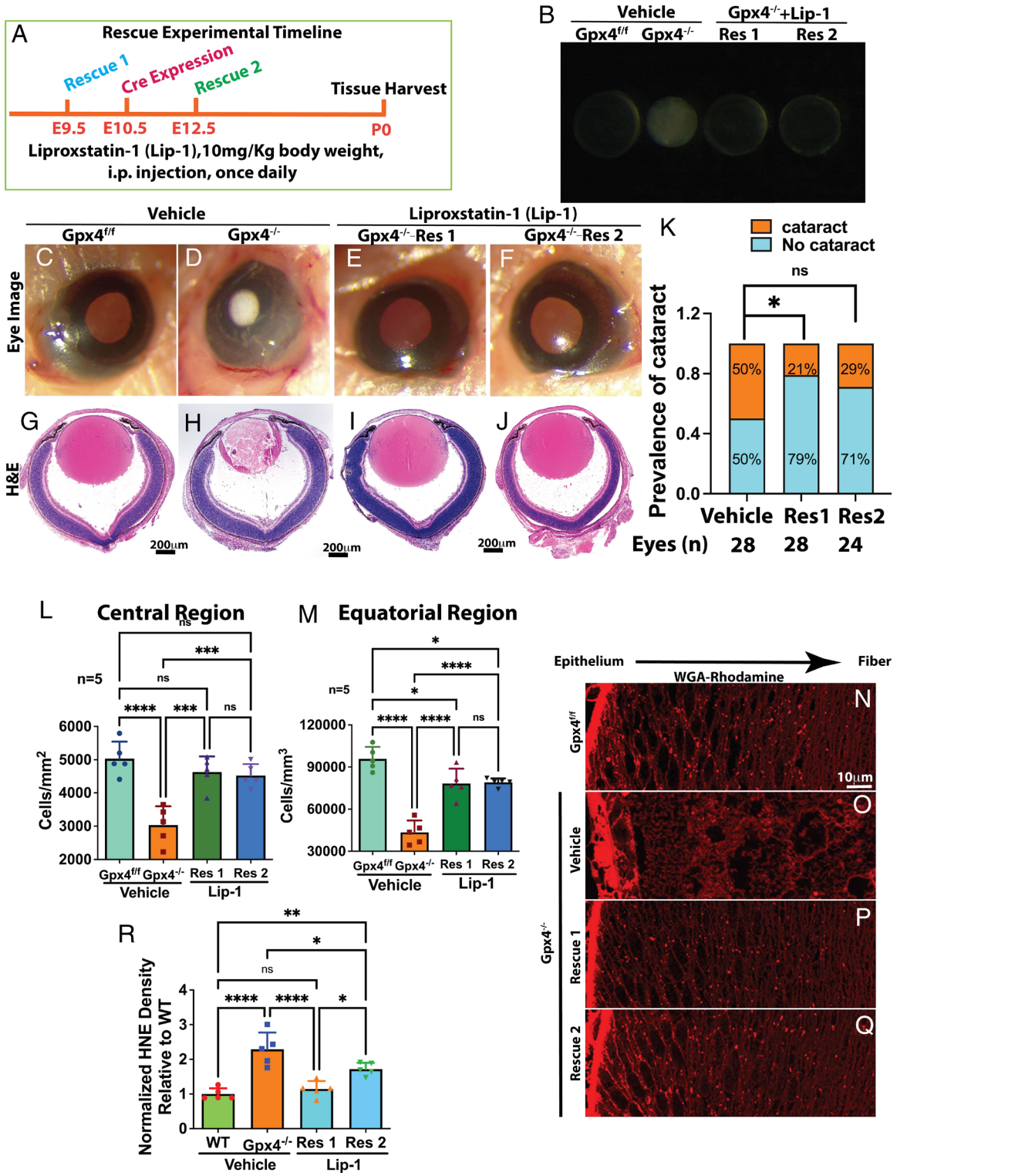

Fig. 5. Blocking lipid peroxidation by Lip-1 attenuates lens development defects. Lip-1, administered at a dosage of 10 mg/kg body weight, was delivered daily to pregnant mothers via intraperitoneal (i.p.) injection starting at E9.5 (rescue 1, Res1) and E12.5 (rescue 2, Res2) as illustrated in (*A*). Analysis was conducted on lenses at P0. (*B*) Darkfield images of lenses revealed that Lip-1 injection at both E9.5 and E12.5 effectively prevented lens opacity. (*C–F*) Slit lamp images of P0 mouse eyes exhibited cataract formation in Gpx4$^{-/-}$ mouse lenses without Lip-1 administration, while both Res1 and Res2 interventions prevented lens opacity. (*G–J*) H&E staining displayed disrupted lens structure in Gpx4$^{-/-}$ mouse lenses without Lip-1 administration, whereas Lip-1 injection at both E9.5 and E12.5 preserved lens fiber cell structure and morphology. (*K*) The efficacy of rescue by Lip-1 administration at E9.5 and E12.5. A chi-square test revealed significant prevention of Gpx4 deficiency-induced lens defects when Lip-1 was administered at E9.5. While a high rate of protection from cataract formation was observed with Lip-1 administered at E12.5, it did not reach statistical significance. (*L*) Cell counts in the central region showed significantly less cell loss in both Res1 and Res2 rescue experiments. (*M*) Cell counts in the equatorial region demonstrated significantly less cell loss in both Res1 and Res2 rescue experiments. (*N*) WGA staining illustrated normal fiber cell alignment comparable to WT mouse lenses (*N*) in both Res1 (*P*) and Res2 (*Q*), whereas lens fiber cell disruption was observed in Gpx4$^{-/-}$ mouse lenses (*O*). (*R*) Both Res1 and Res2 significantly reduced HNE formation compared to Gpx4$^{-/-}$ mouse lenses. All mice with correct Gpx4 KO genotype were used for comparison with control mice. The chi-square test was performed in *K*. One-way ANOVA with Tukey's multiple comparisons test was conducted in *L*, *M*, and *R*. Significance was considered at $P < 0.05$, denoted as *<0.05, **<0.01, ***<0.001, ****<0.0001.

markedly increased lipid peroxidation. TfR1 and ACSL4, recognized ferroptosis markers (47), are elevated in Gpx4 KO lenses compared to WT. However, xCT and FTL, two genes typically involved in protecting cells from ferroptosis, are also upregulated in Gpx4 KO lenses compared to WT. We hypothesize that this represents a part of the cellular stress feedback mechanisms aimed at enhancing GSH production and iron storage due to low intracellular GSH but high intracellular iron levels.

We employed MLR-10 cre to induce lens-specific Gpx4 deletion, initiating cre expression at E10.5. Interestingly, we observed initial cell death and fiber cell degeneration only from E15.5 onward, with no notable pathology evident at E14.5. During the developmental stage, the LEC cycle is considerably shorter compared to the postnatal stage. Sikic et al. (48) reported that the LEC cycle lasts only 8 h (with a 5-h S-phase) at E14.5, contrasting with the 24-h cycle (with a 12-h S-phase) observed in adult mice. The rate of LEC proliferation appears to be even more rapid between E15.5 to E18.5, as indicated by an in vivo ultrasound biomicroscopy study showing a substantial increase in lens volume (approximately fivefold) from E15.5 to E18.5, compared to the increase from E13.5 to E15.5 (around threefold) (49). We speculate that the swift proliferation of LECs from E15.5 to E18.5 demands heightened cellular metabolism and mitochondrial activity, concurrently leading to elevated intracellular oxidation that necessitates increased attention from GPX4 to mitigate lipid peroxidation. More studies are needed to understand the redox status and metabolism in the rapid transition from E14.5 to E18.5.

We observed a significant impact on the morphology and alignment of lens fiber cells in lenses deficient in GPX4, as evidenced by WGA staining in both ex vivo and in vivo studies. In contrast to the typical flat and hexagonal arrangement of fiber cells, lenses lacking GPX4 activity or expression exhibit a predominance of round-shaped fiber cells. Additionally, the characteristic dotted patterns along the fiber cell membrane, indicative of ball-and-socket type interactions, are absent in GPX4 deficiency lenses. This is likely a consequence of compromised permeability of the fiber-cell membrane to polar molecules due to lipid peroxidation-mediated damage. The integrity and functionality of biological membranes hinge on their ability to act as barriers against the permeation of polar molecules (4). The hydrophobic barrier of lipid bilayer membranes, saturated with cholesterol, typically assumes a rectangular shape. Integral membrane proteins, such as aquaporins, major intrinsic proteins, gap junction proteins, and sodium/potassium/calcium exchanger proteins, play crucial roles in modulating the barrier properties of surrounding lipids (50). Damage induced by lipid peroxidation is likely to disrupt the function and stability of these membrane integral proteins, impacting molecular permeability. The infiltration of unselective polar molecules can lead to swelling of fiber cells and ultimately contribute to the formation of cataracts, thus representing one of the mechanisms of cataractogenesis (4, 51). Further investigations are warranted to ascertain whether membrane selective permeability is compromised in GPX4 deficiency lenses, as well as to evaluate the expression and functionality of membrane integral proteins.

The deleterious impact of lipid peroxidation on lens plasma membrane integrity, aberrant lens growth, and cataract formation was substantiated by our rescue experiments involving the administration of a lipid peroxidation inhibitor to pregnant mothers. Notably, the timely provision of Lip-1 significantly mitigated lens developmental abnormalities. Moreover, even when administered at a later stage, Lip-1 showed a beneficial effect on lens maturation. The ability of Lip-1 to effectively prevent lens opacification via intraperitoneal (IP) injection implies its capacity to traverse both the placental and blood–brain barriers.

Collectively, our present study, employing in vitro, ex vivo, and in vivo approaches, elucidates the pivotal role of GPX4 in preserving lens plasma membrane integrity, ensuring appropriate lens development, and shielding the lens from cataractogenesis. GPX4 deficiency in the lens initiates lipid peroxidation, leading to the induction of ferroptosis in LECs, disrupting lens fiber cell alignment, and culminating in cataract formation. Conversely, the provision of a lipid peroxidation inhibitor demonstrates efficacy in preventing lens plasma membrane damage and the onset of cataracts.

Materials and methods

Animals. All animal experiments were conducted in compliance with the protocols approved by the Augusta University Animal Care and Use Committee and adhered to the guidelines outlined in the Association for Research in Vision and Ophthalmology Statement for the Use of Animals in Ophthalmic and Vision Research. Animals were kept under diurnal lighting conditions and provided ad libitum access to food and water. The lens conditional Gpx4 KO ($Gpx4^{-/-}$) mice were generated through crossbreeding between Gpx4 floxed mice ($Gpx4^{f/f}$, Jackson Laboratory, stock# 027964) and MLR-10/Cre mice (52).

Ex Vivo Lens Culture and Treatment. Lenses from 2-mo-old mice were carefully extracted and rinsed three times with 10 mL of Hank's Balanced Salt Solution (HBSS) followed by a single rinse with 10 mL of M199 medium. The lenses were then cultured overnight in M199 medium supplemented with 100 U/mL of penicillin and streptomycin, as well as 2.5 μg/mL of amphotericin B (Cat. 15290026, ThermoFisher). Any opaque lenses were discarded, and only clear lenses were retained for further experimentation. These clear lenses were cultured continuously in M199 medium with or without 10 μM RSL3 for a period of 14 d, with medium renewal every 2 d. After the incubation period, lenses were either fixed with Davidson's fixative for histological analysis or subjected to protein assays.

Cell Culture. The human LEC line, FHL124 cells (53), was provided by Michael Wormstone at the University of East Anglia, UK, and was grown in minimum essential medium (MEM) with 5% fetal bovine serum (FBS), 100 U/mL of penicillin and streptomycin at 35 °C in a humidified 5% CO_2 incubator. Mouse LEC line 17EM15 was provided by Salil Lachke at the University of Delaware and was grown in Dulbecco's modified eagle's medium (DMEM) with 10% FBS, 100 U/mL of penicillin and streptomycin at 37 °C in a humidified 5% CO_2 incubator. HeLa cells and HEK293T cells were also maintained in DMEM with 10% FBS, 100 U/mL of penicillin and streptomycin at 37 °C in a humidified 5% CO_2 incubator.

Creating GPX4 KO FHL124 Cells by CRISPR/Cas9 Editing. The sgRNA was successfully integrated into the lentiCRISPR v2 vector (kindly provided by Feng Zhang, Addgene plasmid #52961). Lentiviral particles were subsequently produced from HEK293T cells by cotransfecting lentiCRISPR v2, VSV-G, BH10 $\phi^{-}env^{-}$, and pRev c as described in our previous study (54). Following this, FHL124 cells were infected with these lentiviral particles and allowed to proliferate for 48 h. The cells stably infected were then selected using 2 μg/mL puromycin. For single-cell expansion, the infected cells were diluted and seeded into a 96-well plate. Validation of individual clonal cell lines with GPX4 deletion was conducted through immunoblot analysis. During selection and regular maintenance, 1 μM Lip-1 was included in the culture medium. Two sets of GPX4 gRNA were employed: GPX4 gRNA1 with the sequence GAATTTGACGTTGTAGCCCG and GPX4 gRNA2 with the sequence TTAACCTGGACAAGTACCGG.

Lip-1 Rescue. Lip-1 was initially dissolved in dimethyl sulfoxide (DMSO) at a concentration of 25 mg/mL and subsequently diluted with corn oil (Cat. 405435000, ThermoFisher) to a final concentration of 2.5 mg/mL. A dosage of 10 mg/kg body weight was administered. For vehicle treatment, a similar volume of DMSO and corn oil was utilized. Female mice aged 2 mo were selected for breeding. At E9.5 and E12.5, Lip-1 or vehicle was administered daily via intraperitoneal (i.p.) injection. Lenses of the litters born on the same day were examined as described.

Statistical Analysis. All data are presented as mean ± SD, and statistical analyses were performed using two-tailed Student's *t* test, One-way ANOVA, or Chi-square test as described in each figure. A *P*-value below 0.05 was considered significant.

The degree of significance is denoted by the following symbols: $*P < 0.05$, $**P < 0.01$, $***P < 0.001$, $****P < 0.0001$.

Other Methods. Please see other methods in *SI Appendix*.

Data, Materials, and Software Availability. All lipidomics data were deposited in Metabolomics Workbench (datatrack_id:5072, and study_id:ST003407), DOI: 10.21228/M80V5D (55). Other data needed to evaluate the conclusions in the paper are presented in the paper and/or *SI Appendix*.

ACKNOWLEDGMENTS. This research was suppxorted by grants from EY028158 (X.F.), EY032488 (X.F.), the James Fickel Alzheimer's Disease Research Fund MCGFD01043 (X.F.), and National Eye Institute (NEI) Center Core Grant for Vision Research (P30EY031631) at Augusta University. NIH Common Fund's National Metabolomics Data Repository. We extend our gratitude to team at Integrated Lipidomics and Metabolomics Core Laboratory at Emory School of Medicine for their help in lipidomics. We are very grateful to Dr. Brendan Marshall, Tania Green, and Libby Perry at Augusta University EM and Histology Core for their help in transmission electron microscopy (TEM) experiment.

Author affiliations: [a]Department of Cellular Biology and Anatomy, Medical College of Georgia at Augusta University, Augusta, GA 30912; [b]Department of Pathology and Biological Responses, Nagoya University Graduate School of Medicine, Nagoya, Aichi 464-0083, Japan; and [c]School of Medicine, Emory Integrated Metabolomics and Lipidomics Core, Emory University, Atlanta, GA 30322

1. Z. Liu *et al.*, The lens epithelium as a major determinant in the development, maintenance, and regeneration of the crystalline lens. *Prog. Retin. Eye Res.* **92**, 101112 (2023).
2. N. A. Delamere, S. Tamiya, Expression, regulation and function of Na, K-ATPase in the lens. *Prog. Retin. Eye Res.* **23**, 593–615 (2004).
3. S. Rowan, M. L. Chang, N. Reznikov, A. Taylor, Disassembly of the lens fiber cell nucleus to create a clear lens: The p27 descent. *Exp. Eye Res.* **156**, 72–78 (2017).
4. J. Kistler, S. Bullivant, Structural and molecular biology of the eye lens membranes. *Crit. Rev. Biochem. Mol. Biol.* **24**, 151–181 (1989).
5. W. K. Subczynski, L. Mainali, M. Raguz, W. J. O'Brien, Organization of lipids in fiber-cell plasma membranes of the eye lens. *Exp. Eye Res.* **156**, 79–86 (2017).
6. P. S. Zelenka, Lens lipids. *Curr. Eye Res.* **3**, 1337–1359 (1984).
7. G. O. Fruhwirth, A. Loidl, A. Hermetter, Oxidized phospholipids: From molecular properties to disease. *Biochim. Biophys. Acta* **1772**, 718–736 (2007).
8. L. Huang, R. Estrada, M. C. Yappert, D. Borchman, Oxidation-induced changes in human lens epithelial cells. 1. Phospholipids. *Free Radic. Biol. Med.* **41**, 1425–1432 (2006).
9. J. R. Hughes *et al.*, Instability of the cellular lipidome with age. *Age (Dordr)* **34**, 935–947 (2012).
10. M. A. Babizhayev, Failure to withstand oxidative stress induced by phospholipid hydroperoxides as a possible cause of the lens opacities in systemic diseases and ageing. *Biochim. Biophys. Acta* **1315**, 87–99 (1996).
11. D. Borchman, M. C. Yappert, Age-related lipid oxidation in human lenses. *Invest. Ophthalmol. Vis. Sci.* **39**, 1053–1058 (1998).
12. F. Ursini, M. Maiorino, M. Valente, L. Ferri, C. Gregolin, Purification from pig liver of a protein which protects liposomes and biomembranes from peroxidative degradation and exhibits glutathione peroxidase activity on phosphatidylcholine hydroperoxides. *Biochim. Biophys. Acta* **710**, 197–211 (1982).
13. M. Maiorino *et al.*, Distinct promoters determine alternative transcription of gpx-4 into phospholipid-hydroperoxide glutathione peroxidase variants. *J. Biol. Chem.* **278**, 34286–34290 (2003).
14. F. P. Bellinger *et al.*, Glutathione peroxidase 4 is associated with neuromelanin in substantia nigra and dystrophic axons in putamen of Parkinson's brain. *Mol. Neurodegener.* **6**, 8 (2011).
15. Y. Zou *et al.*, A GPX4-dependent cancer cell state underlies the clear-cell morphology and confers sensitivity to ferroptosis. *Nat. Commun.* **10**, 1617 (2019).
16. T. Tadokoro *et al.*, Mitochondria-dependent ferroptosis plays a pivotal role in doxorubicin cardiotoxicity. *JCI Insight* **5**, e132747 (2020).
17. J. Zhang *et al.*, Involvement of GPX4 in irisin's protection against ischemia reperfusion-induced acute kidney injury. *J. Cell Physiol.* **236**, 931–945 (2021).
18. H. Imai *et al.*, Early embryonic lethality caused by targeted disruption of the mouse PHGPx gene. *Biochem. Biophys. Res. Commun.* **305**, 278–286 (2003).
19. Z. Wei *et al.*, Aging lens epithelium is susceptible to ferroptosis. *Free Radic. Biol. Med.* **167**, 94–108 (2021).
20. D. Y. Ma *et al.*, GSK-3beta-dependent Nrf2 antioxidant response modulates ferroptosis of lens epithelial cells in age-related cataract. *Free Radic. Biol. Med.* **204**, 161–176 (2023).
21. Y. Wang *et al.*, Lens epithelium cell ferroptosis mediated by m(6)A-lncRNA and GPX4 expression in lens tissue of age-related cataract. *BMC Ophthalmol.* **23**, 514 (2023).
22. X. Zhang, C. Zheng, J. Zhao, X. Xu, J. Yao, LncRNA MEG3 regulates ferroptosis of lens epithelial cells via PTBP1/GPX4 axis to participate in age-related cataract. *J. Cell Physiol.*, 10.1002/jcp.31330 (2024).
23. F. Ursini, M. Maiorino, Lipid peroxidation and ferroptosis: The role of GSH and GPx4. *Free Radic. Biol. Med.* **152**, 175–185 (2020).
24. Z. Wei *et al.*, Mitotic activation around wound edges and epithelialization repair in UVB-induced capsular cataracts. *Invest. Ophthalmol. Vis. Sci.* **62**, 29 (2021).
25. H. Zheng, L. Jiang, T. Tsuduki, M. Conrad, S. Toyokuni, Embryonal erythropoiesis and aging exploit ferroptosis. *Redox Biol.* **48**, 102175 (2021).
26. D. B. Gutierrez, D. L. Garland, J. H. Schwacke, D. L. Hachey, K. L. Schey, Spatial distributions of phosphorylated membrane proteins aquaporin 0 and MP20 across young and aged human lenses. *Exp. Eye Res.* **149**, 59–65 (2016).
27. J. Gao, P. J. Minogue, E. C. Beyer, R. T. Mathias, V. M. Berthoud, Disruption of the lens circulation causes calcium accumulation and precipitates in connexin mutant mice. *Am. J. Physiol. Cell Physiol.* **314**, C492–C503 (2018).
28. E. Wang, A. Geng, A. M. Maniar, B. W. Mui, X. Gong, Connexin 50 regulates surface ball-and-socket structures and fiber cell organization. *Invest. Ophthalmol. Vis. sci.* **57**, 3039–3046 (2016).
29. C. G. Baumann *et al.*, Lipid differentiation in MP26 junction enriched membranes of bovine lens fiber cells. *Biochim. Biophys. Acta* **1303**, 145–153 (1996).
30. C. R. Fleschner, R. J. Cenedella, Lipid composition of lens plasma membrane fractions enriched in fiber junctions. *J. Lipid Res.* **32**, 45–53 (1991).
31. J. Alcala, M. Katar, H. Maisel, Lipid composition of chick lens fiber cell gap junctions. *Curr. Eye Res.* **2**, 569–578 (1982).
32. J. A. Flores *et al.*, Connexin-46/50 in a dynamic lipid environment resolved by CryoEM at 1.9 A. *Nat. Commun.* **11**, 4331 (2020).
33. T. Gonen *et al.*, Lipid-protein interactions in double-layered two-dimensional AQP0 crystals. *Nature* **438**, 633–638 (2005).
34. S. Scheuring *et al.*, Structural models of the supramolecular organization of AQP0 and connexons in junctional microdomains. *J. Struct. Biol.* **160**, 385–394 (2007).
35. P. V. Usatyuk, V. Natarajan, Hydroxyalkenals and oxidized phospholipids modulation of endothelial cytoskeleton, focal adhesion and adherens junction proteins in regulating endothelial barrier function. *Microvasc. Res.* **83**, 45–55 (2012).
36. A. Ayala, M. F. Munoz, S. Arguelles, Lipid peroxidation: Production, metabolism, and signaling mechanisms of malondialdehyde and 4-hydroxy-2-nonenal. *Oxid Med. Cell Longev.* **2014**, 360438 (2014).
37. M. C. Oliveira, R. M. Cordeiro, A. Bogaerts, Effect of lipid oxidation on the channel properties of Cx26 hemichannels: A molecular dynamics study. *Arch. Biochem. Biophys.* **746**, 109741 (2023).
38. T. F. L. Wishart, M. Flokis, D. Y. Shu, S. J. Das, F. J. Lovicu, Hallmarks of lens aging and cataractogenesis. *Exp. Eye Res.* **210**, 108709 (2021).
39. J. A. Whitson *et al.*, Transcriptome of the GSH-depleted lens reveals changes in detoxification and EMT signaling genes, transport systems, and lipid homeostasis. *Invest. Ophthalmol. Vis. Sci.* **58**, 2666–2684 (2017).
40. K. Varadaraj, J. Gao, R. T. Mathias, S. S. Kumari, GPX1 knockout, not catalase knockout, causes accelerated abnormal optical aberrations and cataract in the aging lens. *Mol. Vis.* **28**, 11–20 (2022).
41. V. N. Reddy *et al.*, Glutathione peroxidase-1 deficiency leads to increased nuclear light scattering, membrane damage, and cataract formation in gene-knockout mice. *Invest. ophthalmol. Vis. Sci.* **42**, 3247–3255 (2001).
42. M. F. Lou, Glutathione and glutaredoxin in redox regulation and cell signaling of the lens. *Antioxidants (Basel)* **11**, 1973 (2022).
43. J. V. Fecondo, R. C. Augusteyn, Superoxide dismutase, catalase and glutathione peroxidase in the human cataractous lens. *Exp. Eye Res.* **36**, 15–23 (1983).
44. K. C. Bhuyan, D. K. Bhuyan, Superoxide dismutase of the eye: Relative functions of superoxide dismutase and catalase in protecting the ocular lens from oxidative damage. *Biochim. Biophys. Acta* **542**, 28–38 (1978).
45. M. Maiorino *et al.*, Phospholipid hydroperoxide glutathione peroxidase is the 18-kDa selenoprotein expressed in human tumor cell lines. *J. Biol. Chem.* **266**, 7728–7732 (1991).
46. J. P. Thomas, M. Maiorino, F. Ursini, A. W. Girotti, Protective action of phospholipid hydroperoxide glutathione peroxidase against membrane-damaging lipid peroxidation. In situ reduction of phospholipid and cholesterol hydroperoxides. *J. Biol. Chem.* **265**, 454–461 (1990).
47. H. Feng *et al.*, Transferrin receptor is a specific ferroptosis marker. *Cell Rep.* **30**, 3411–3423.e7 (2020).
48. H. Sikic, Y. Shi, S. Lubura, S. Bassnett, A full lifespan model of vertebrate lens growth. *R Soc. Open Sci.* **4**, 160695 (2017).
49. F. S. Foster, M. Zhang, A. S. Duckett, V. Cucevic, C. J. Pavlin, In vivo imaging of embryonic development in the mouse eye by ultrasound biomicroscopy. *Invest. Ophthalmol. Vis. Sci.* **44**, 2361–2366 (2003).
50. R. T. Mathias, T. W. White, X. Gong, Lens gap junctions in growth, differentiation, and homeostasis. *Physiol. Rev.* **90**, 179–206 (2010).
51. H. V. Brooks, R. D. Jolly, C. A. Paterson, The pathology of an inherited cataract of sheep. *Curr. Eye Res.* **2**, 625–632 (1982).
52. H. Zhao, Y. Yang, C. M. Rizo, P. A. Overbeek, M. L. Robinson, Insertion of a Pax6 consensus binding site into the alphaA-crystallin promoter acts as a lens epithelial cell enhancer in transgenic mice. *Invest. Ophthalmol. Vis. Sci.* **45**, 1930–1939 (2004).
53. J. R. Reddan *et al.*, Generation of two non-transfected human lens cell lines. *Invest. Ophthalmol. Vis. Sci.* **40**, S970–S970 (1999).
54. J. Huangfu *et al.*, Cellular FLICE-like inhibitory protein (cFLIP) critically maintains apoptotic resistance in human lens epithelial cells. *Cell Death Dis.* **12**, 386 (2021).
55. X. Fan, Deficiency in glutathione peroxidase 4 (GPX4) results in abnormal lens development and newborn cataract. Metabolomics Workbench. http://dx.doi.org/10.21228/M80V5D. Deposited 8 January 2024.